Eliminating Leakage Currents in Neutral Point Clamped Inverters for Photovoltaic Systems

Marcelo C. Cavalcanti, Alexandre M. Farias, *Student Member, IEEE*, Kleber C. Oliveira, Francisco A. S. Neves, *Member, IEEE*, and João L. Afonso, *Member, IEEE*

Abstract—The main contribution of this paper is the proposal of new modulation techniques for three-phase transformerless neutral point clamped inverters to eliminate leakage currents in photovoltaic systems without requiring any modification on the multilevel inverter or any additional hardware. The modulation techniques are capable of reducing the leakage currents in photovoltaic systems by applying three medium vectors or using only two medium vectors and one specific zero vector to compose the reference vector. In addition, to increase the system utilization, the three-phase neutral point clamped inverter can be designed to also provide functions of active filter using the p–q theory. The proposed system provides maximum power point tracking and compensation of current harmonics and reactive power. To validate the simulation models, an experimental three-phase inverter is used to evaluate leakage currents and the dc link voltage control.

Index Terms—Energy conversion, photovoltaic power systems, pulse width modulated power converters.

I. INTRODUCTION

IN RECENT YEARS, the increasing demand for energy has stimulated the development of alternative power sources such as photovoltaic (PV) modules, fuel cells, and wind turbines. The PV modules are particularly attractive as renewable sources due to their relative small size, noiseless operation, simple installation, and to the possibility of installing them closer to the user.

In PV modules, the output voltage has a low dc amplitude value. In order to be connected to the grid, the PV modules output voltage should be boosted and converted into an ac voltage. This task can be performed using one or more conversion stages (multi-stage). Many topologies for PV systems are multi-stage, having a dc-dc converter with a high-frequency transformer that adjusts the inverter dc voltage and isolates the PV modules from the grid [1]–[3]. However, the conversion stages decrease the efficiency and make the system more complex [4]. The transformerless centralized configuration with one-stage technology uses only one inverter and a large number of series-connected PV modules, called strings, are used in order to generate sufficient voltage to connect to the grid [5]. In PV systems where series modules are connected to a conventional two-level inverter, the occurrence of partial shades and the mismatching of the modules lead to a reduction of the generated power [6], [7]. To overcome these problems, the connection of the modules can be made using a multilevel converter [8]–[11]. The multilevel converter maximizes the power obtained from the arrays, reduces the device voltage stress, and generates output voltages with lower total harmonic distortion (THD) [8].

Avoiding transformers is a benefit of multilevel inverters and normally neutral point clamped (NPC) inverters are not used with transformers. However, in PV applications, the transformerless systems have problems related to leakage currents, thus it is necessary to pay special attention to this issue.

The main disadvantage of the topologies without transformer is the connection of the PV array to the grid without galvanic isolation. Thus, the fluctuations in the potential between the PV array and ground give rise to capacitive leakage current and these currents can cause grid current distortion and losses in the system. Three-phase two-level inverters are not suitable for transformerless PV applications because of the high leakage currents that appear due to the conventional pulse-width-modulation (PWM) [9].

On the other hand, power electronic converters can also be connected to the grid for improving the system power quality. Working as active filter (AF) [12], they can perform harmonic and reactive power compensation. For this reason, it is convenient to integrate both functionalities of power generation and power quality improvement using the same hardware structure presented in the distributed generation system. A theory for the control of AF in three-phase power systems, called p–q theory, was proposed in [13]. The theory was initially developed for three-phase three-wire systems, with a brief mention to systems with neutral wire. Later, the theory was extended to three-phase four-wire systems [14], [15].

In this paper, PWM techniques for three-phase NPC inverters are proposed to eliminate the leakage current in transformerless PV systems without requiring any modification on the NPC inverter or any additional hardware. Furthermore, the NPC inverter is studied for PV systems with function of AF using the p–q theory to increase the system utilization. The paper is organized as follows: in Section II, common-mode voltages (CMV) and leakage currents in three-level inverters are
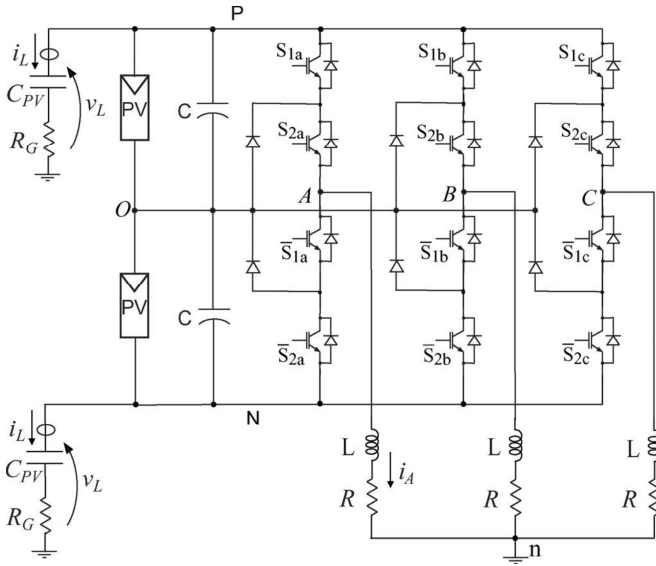
Fig. 1. Three-phase NPC inverter to evaluate leakage currents.

analyzed. The conventional PWM for three-phase NPC inverters is discussed in Section III. In Section IV, modulation techniques for three-phase NPC inverters are proposed in order to eliminate the leakage current in transformerless PV systems. In Section V, NPC inverters with different modulation techniques for three-phase systems are compared based on the leakage currents. Experimental results are presented to prove the effect of the common-mode voltage on the leakage currents. The dc link voltage control using the proposed PWM is presented in Section VI. In order to validate the control system for the NPC inverter, the NPC is tested and experimental results are presented. In Section VII, the three-phase NPC inverter with additional function of AF using the p–q theory is discussed. The AF function of the NPC inverter is verified through simulations. Conclusions are presented in Section VIII.

II. COMMON-MODE VOLTAGES IN PHOTOVOLTAIC INVERTERS

In transformerless grid connected PV systems, there is a connection between the grid and the dc source and thus, a leakage current appears through a circuit that is created if the PV array is grounded [4]. The leakage current can reach high values therefore becoming an important issue in transformerless PV systems.

It is possible to express the voltages between the positive (P) or negative (N) dc bus and the neutral (n) $(V_{Pn}$ or $V_{Nn})$ in terms of the inverter output voltages

$$V_{Nn} = V_{kn} - V_{kN} \tag{1}$$

$$V_{Pn}V_{Pn} = V_{kn} - V_{kP} = V_{kn} - (V_{kN} - V_{PN}) \tag{2}$$

where $k = A, B, C$ (Fig. 1).

Under balanced operation, the following condition for the inverter voltages can be written:
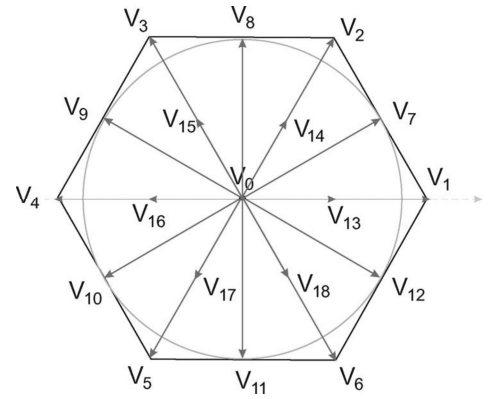
$$V_{An} + V_{Bn} + V_{Cn} = 0. \tag{3}$$

Fig. 2. Space vectors in the output of a three-level inverter.

Using (1)–(3)

$$V_{Nn} = -\frac{V_{AN} + V_{BN} + V_{CN}}{3} \tag{4}$$

$$V_{Pn} = V_{PN} - \frac{V_{AN} + V_{BN} + V_{CN}}{3}. \tag{5}$$

The CMV for the three-phase inverter can be calculated as

$$V_{CM} = \frac{V_{AN} + V_{BN} + V_{CN}}{3}. \tag{6}$$

The voltage V_{Nn} is the negative of the CMV and the voltage V_{Pn} is $V_{PN} + V_{Nn}$. Therefore, the leakage currents can be attenuated by the control of the CMV.

III. SPACE VECTOR MODULATION

The space vector PWM (SVPWM) is generally used to control the three-level inverter output voltages (Fig. 1) and there are 19 possible space vectors as shown in Fig. 2: one zero vector (V_0) with three switching possibilities, six long vectors $(V_1, V_2, V_3, V_4, V_5,$ and $V_6)$, six medium vectors $(V_7, V_8, V_9, V_{10}, V_{11},$ and $V_{12})$ and six small vectors $(V_{13}, V_{14}, V_{15}, V_{16}, V_{17},$ and $V_{18})$ with two switching possibilities each, which total to 27 possible switching combinations. Table I presents the switches states for obtaining the space vectors located in the region from $-30°$ to $150°$ of the α–β plane. The complete table is not presented due to space restrictions. The corresponding CMV are also presented.

The maximum amplitude of the phase-to-neutral voltages is $V_{PN}/\sqrt{3}(m = 1)$ in the linear region, where the modulation index is defined as

$$m = \frac{\sqrt{3}V_{kn}^*}{V_{PN}} \tag{7}$$

and V_{kn}^* is the reference amplitude of the phase-to-neutral voltages.

Depending on the choice of which space vectors are used to produce the phase reference voltages, the CMV may vary during the switching period. For example, for a reference voltage vector in the first 30°, with $m > 0.5$, one could use the vectors $V_1, V_7,$ and V_{13}. It can be seen in Table I that using SVPWM, the CMV changes every time a different space vector

TABLE I
CORRESPONDING SPACE VECTOR FOR THE POSSIBLE COMBINATIONS OF
THE INVERTER SWITCHES FROM $-30°$ TO $150°$

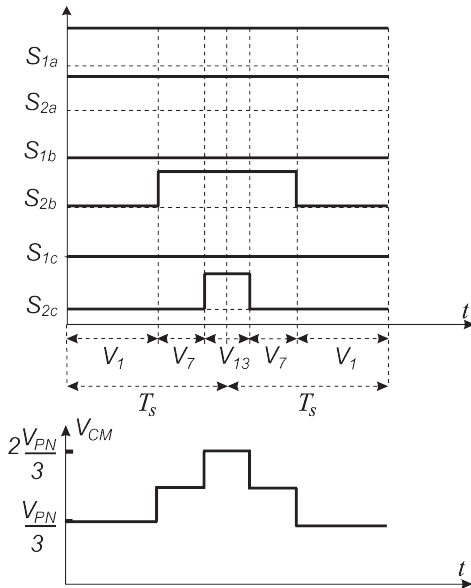| S_{1a}	S_{2a}	S_{1b}	S_{2b}	S_{1c}	S_{2c}	Vector	V_{CM}
0	0	0	0	0	0	V_0	0
1	1	1	1	1	1	V_0	V_{PN}
0	1	0	1	0	1	V_0	$V_{PN}/2$
1	1	0	0	0	0	V_1	$V_{PN}/3$
1	1	1	1	0	0	V_2	$2V_{PN}/3$
0	0	1	1	0	0	V_3	$V_{PN}/3$
1	1	0	1	0	0	V_7	$V_{PN}/2$
0	1	1	1	0	0	V_8	$V_{PN}/2$
0	0	1	1	0	1	V_9	$V_{PN}/2$
1	1	0	0	0	1	V_{12}	$V_{PN}/2$
0	1	0	0	0	0	V_{13}	$V_{PN}/6$
1	1	0	1	0	1	V_{13}	$2V_{PN}/3$
0	1	0	1	0	0	V_{14}	$V_{PN}/3$
1	1	1	1	0	1	V_{14}	$5V_{PN}/6$
0	0	0	1	0	0	V_{15}	$V_{PN}/6$
0	1	1	1	0	1	V_{15}	$2V_{PN}/3$

Fig. 3.   Switching pattern and CMV (V_{CM}) for the SVPWM.

is used. Therefore, the CMV assumes three values: $V_{PN}/3$, $V_{PN}/2$, and $2V_{PN}/3$ as shown in Fig. 3.

IV. MODULATION TECHNIQUES TO ELIMINATE LEAKAGE CURRENTS IN THREE-LEVEL INVERTERS

In this section, modulation techniques for three-phase NPC inverters are proposed to eliminate the leakage current in transformerless PV systems.

A. PWM With Three Medium Vectors

Studying the vector space for the NPC three-level inverter, it is possible to define some vector combinations that are capable of reducing the leakage currents in PV systems. The first alternative is applying the three medium vectors (3MV) nearest to the reference. Therefore, if the reference voltage vector is in the region between vectors V_1 and V_2 (0° to 60°), vectors
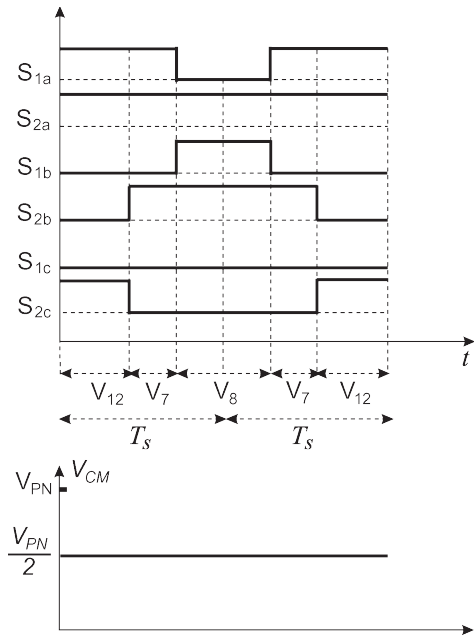

Fig. 4.   Switching pattern and CMV (V_{CM}) for the 3MV.

TABLE II
SWITCHING PATTERNS FOR PWM TECHNIQUES

Techniques	0° to 30°	30° to 60°	60° to 90°
SVPWM	1-7-13-7-1	7-14-2-14-7	2-14-8-14-2
3MV	12-7-8-7-12	12-7-8-7-12	7-8-9-8-7
3MV120	12-8-10-8-12	12-8-10-8-12	7-9-11-9-7
2MV1Z	12-7-0-7-12	7-8-0-8-7	7-8-0-8-7

V_{12}, V_7, and V_8 are used. The switching pattern for the 3MV is shown in Fig. 4.

The differences between the SVPWM and 3MV are illustrated in Table II, for reference voltage vectors located from 0° to 90° (Fig. 2). It can be seen in Table I that using SVPWM, the CMV will change with high frequency. The vectors of the SVPWM were chosen considering $m > 0.5$.

In Fig. 5, it is possible to note that in the linear region, the maximum amplitude of the 3MV [continuous circle in Fig. 5(a)] is lower than the maximum amplitude of the SVPWM [dotted circle in Fig. 5(a)].

The minimum voltage amplitude for this alternative is limited. Therefore, if the amplitude of the phase-to-neutral voltages is lower than $V_{PN}/3$, a variation of the technique is used, with 3MV displaced 120° (3MV120), as shown in Fig. 5(b) for the possible configurations. The 3MV120 presents half of the maximum amplitude that could be obtained using 3MV. In this case, V_{12}, V_8, and V_{10} are used in sectors I, III, and V and V_7, V_9, and V_{11} are used in sectors II, IV, and VI (Fig. 5(b), Table II). The 3MV120 presents two switchings in each vector change, having higher switching losses than the 3MV, being an alternative that could be avoided if the inverter control operates with $m > 0.5$.

B. PWM With Two Medium and One Zero Vectors

The second alternative consists of using only the medium vectors and the zero vector with $V_{CM} = V_{PN}/2$ (2MV1Z)
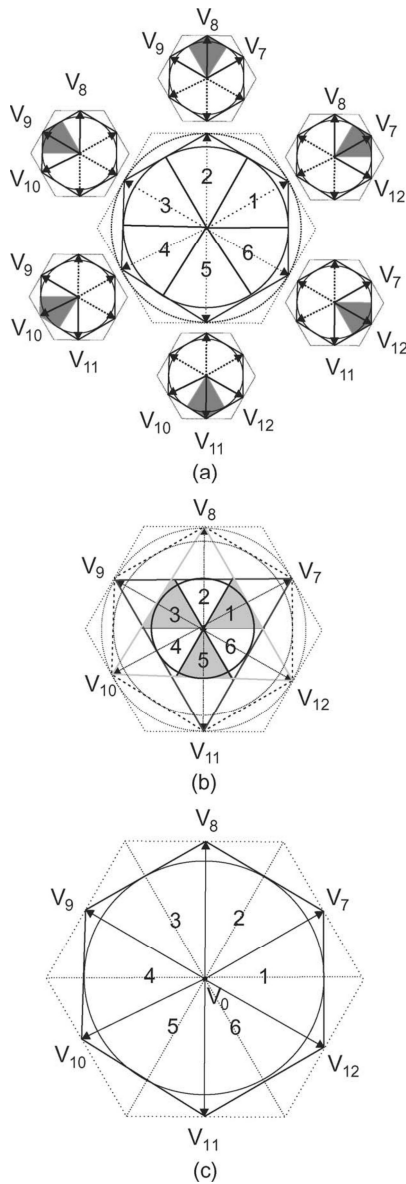
Fig. 5. Vectorial space using (a) 3MV, (b) 3MV120, and (c) 2MV1Z.

Fig. 6. Switching patterns and CMV (V_{CM}) for the 2MV1Z.

to compose the reference vector [Fig. 5(c)]. Considering the region between vectors V_{12} and V_7 ($-30°$ to $30°$), the vectors V_{12}, V_7, and V_0 (with $V_{CM} = V_{PN}/2$) are used. In any option, it can be seen that the CMV always assumes the value $V_{PN}/2$. The switching pattern for the 2MV1Z is shown in Fig. 6.

For the NPC three-level inverters, the 3MV and 2MV1Z can be applied with the maximum amplitude of the phase-to-neutral voltages equal to $V_{PN}/2$, resulting in 86.6% of the voltages that can be obtained with the SVPWM ($V_{PN}/\sqrt{3}$).

C. PWM With Long and Small Vectors

Another alternative is to use combinations of long and small vectors that present the same CMV. In Fig. 2 and Table I, it is possible to verify that the maximum amplitude voltage is $V_{PN}/3$. Then, this option is not the best alternative to be implemented.
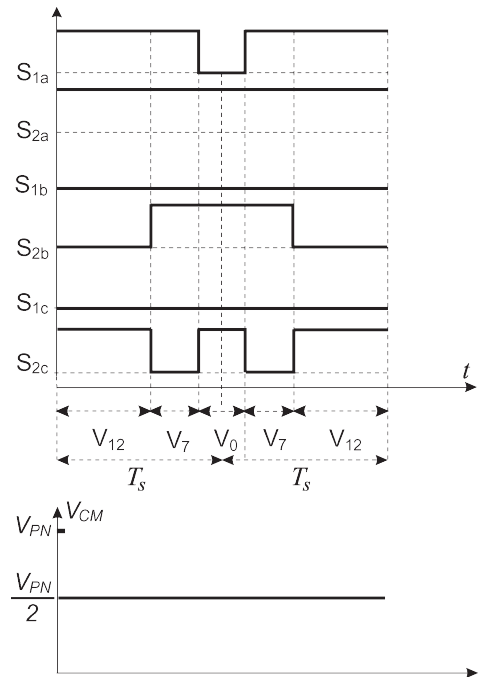
A last alternative is a combination of two techniques (3MV-3MV120-2MV1Z and long-small vectors), with changes between them each at 15°. The gain of this alternative in terms of maximum output voltage in comparison with the techniques that use medium vectors is 3.5%. However, this alternative is implemented with a higher computational effort than the techniques using medium vectors. Therefore, in this paper, 3MV and 2MV1Z are chosen for further investigation.

V. COMPARATIVE ANALYSIS

In this section, the proposed modulation techniques (3MV and 2MV1Z) for three-phase transformerless NPC inverters are used to validate the proposal of eliminating the leakage current in photovoltaic systems. Transformerless PV three-phase inverters (Fig. 1) using different PWM techniques are compared based on the output voltages amplitude (maximum m), CMV, and leakage currents. The simulation parameters are switching period $T_s = 200$ μs, dead time $t_d = 3.5$ μs, fundamental frequency $f = 60$ Hz, load inductance $L = 11.4$ mH, load resistance $R = 16$ Ω, dc link capacitance $C = 2.35$ mF, dc link voltage $V_{PN} = 240$ V, modulation index $m = 0.6$, parasitic capacitance $C_{PV} = 220$ nF, and ground resistance $R_G = 7.5$ Ω. The 3MV and 2MV1Z are compared to the single-phase multilevel modulator, called 1 DM [16]. The 1 DM technique is presented as a general solution to modulate any converter. The modulation problem is reduced to simple calculations while determining the switching sequence and the corresponding switching times. The 1 DM technique can be applied independently to the three phases and can provide null CMV in average. However, for transformerless PV applications, it is necessary to keep the CMV constant to reduce the leakage currents.
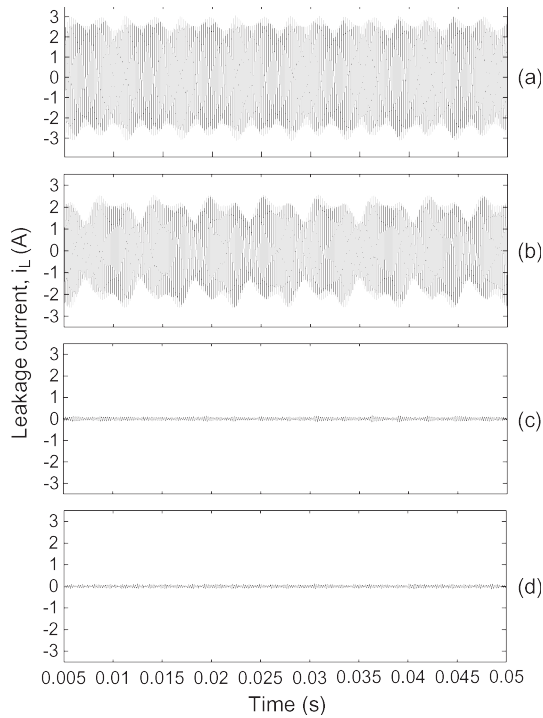
Fig. 7. Simulated leakage current (i_L) of the three-level PV inverter: (a) SVPWM, (b) 1DM, (c) 3MV, and (d) 2MV1Z.

Fig. 8. Simulated output voltage (v_{AO}) and load current (i_A) in phase a for (a) SVPWM, (b) 1DM, (c) 3MV, and (d) 2MV1Z.

TABLE III
COMPARISON OF TRANSFORMERLESS THREE-PHASE INVERTERS

PWM	SVPWM	1DM	3MV	2MV1Z
Maximum m	1	1	0.866	0.866
CMV	variable	variable	constant	constant
Leakage current	>300mA	>300mA	<300mA	<300mA
Current THD	2.67	1.77	1.75	1.39

Simulation results for the leakage currents (i_L in Fig. 1) are presented in Fig. 7 for different PWM techniques. The results in Fig. 7 show that using the proposed PWM, the three-level inverters present low leakage currents in transformerless PV systems. Fig. 8 shows the results for the inverter output voltage and load current in phase a (v_{AO} and i_A in Fig. 1).

The comparison is shown in Table III. Using SVPWM or 1 DM, the CMV jumps between different levels with a high frequency resulting in high leakage currents. In Table III, 300 mA is used as the reference rms value due to German Standard. The THD is defined as

$$\text{THD} = \sqrt{\frac{\sum_{h=2}^{\infty} F_h^2}{F_1^2}} 100\% \qquad (8)$$

where F_h is the rms value of each frequency component of the inverter output current. It can be seen that the THD of the inverter output currents are similar for all PWM techniques.

For the experimental measurements the three-phase setup shown in Fig. 1 was implemented. The prototype parameters are equal to those used in simulation. The complete control system was executed in discrete-time using a digital signal processor
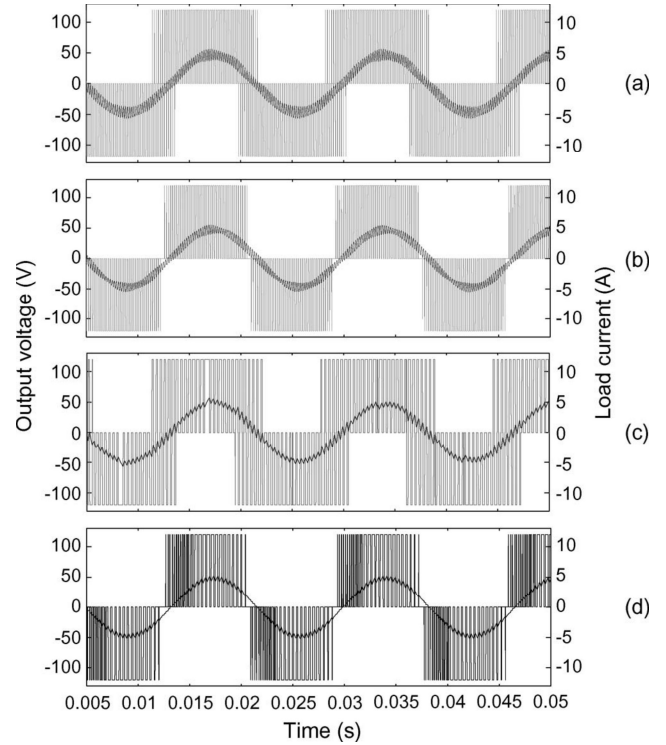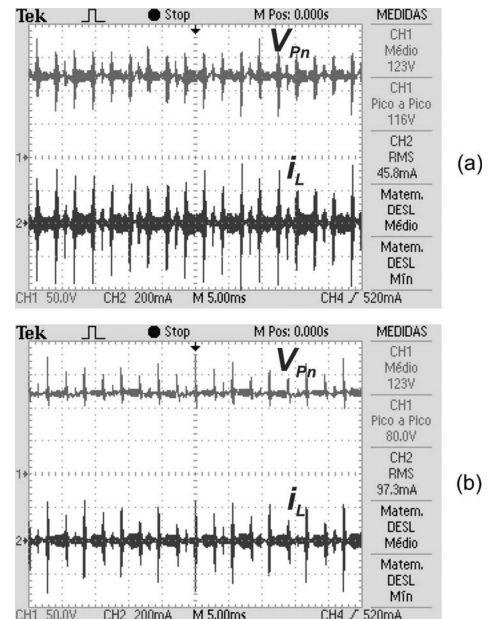

Fig. 9. Experimental voltage v_{Pn} and leakage current (i_L) of the three-level PV inverter: (a) 3MV and (b) 2MV1Z.

with sampling and switching frequencies of 5 kHz. It can be seen in Fig. 9 that the 3MV and 2MV1Z techniques make the leakage current to have low values. The results indicate that the proposed techniques have potential to use in grid connected transformerless three-phase PV systems. Fig. 10 shows the inverter output voltage and load current in phase a for 3MV and 2MV1Z techniques.
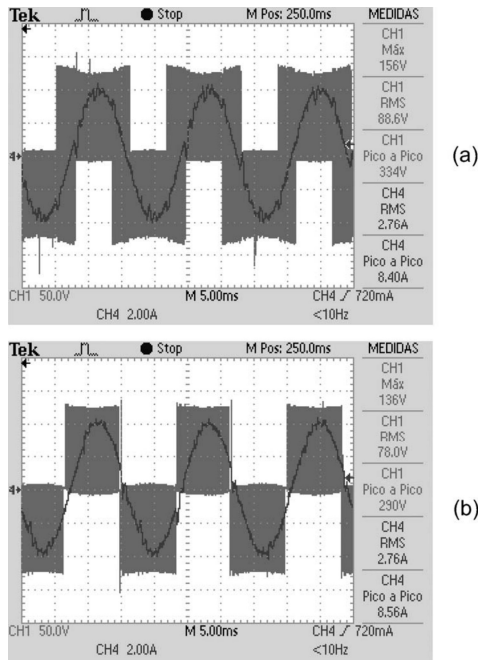
Fig. 10. Experimental output voltage (v_{AO}) and load current (i_A) in phase a for (a) 3MV and (b) 2MV1Z.
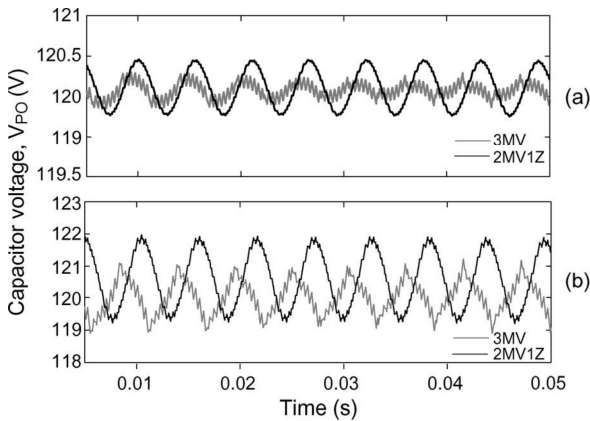

Fig. 11. DC link top capacitor voltage for load resistance (a) $R = 16\ \Omega$ and (b) $R = 4\ \Omega$.

VI. INDEPENDENT DC LINK CAPACITORS VOLTAGE CONTROL

The control using medium vectors is the best choice to achieve low leakage currents in the PV array using the NPC inverter, but these vectors cause dc link capacitors imbalance. Considering a sinusoidal load current, the dc link voltage can be controlled by using 3MV combined with 3MV120 and 2MV1Z. The two combinations of three medium vectors are necessary because of the limitation of voltage amplitude described in Section IV-A. If the voltage amplitude is lower than $V_{PN}/3$, 3MV120 is used, otherwise 3MV is used. As it can be seen in Fig. 11, where the fundamental frequency is $f = 60$ Hz, the dc link top capacitor voltage (V_{PO} in Fig. 1) has a frequency of three times the fundamental and the total dc link voltage is kept in $V_{PN} = 240$ V. The parameters are equal to those used for simulation in Section V. The simulation performed
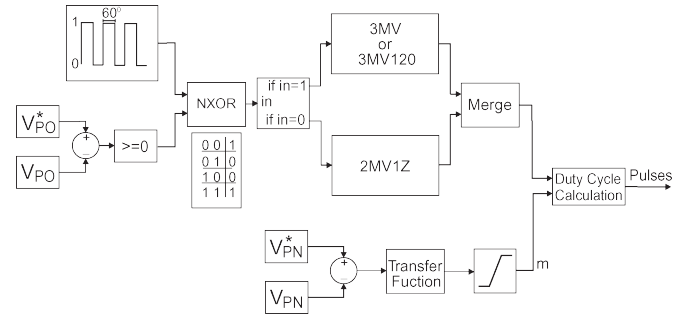

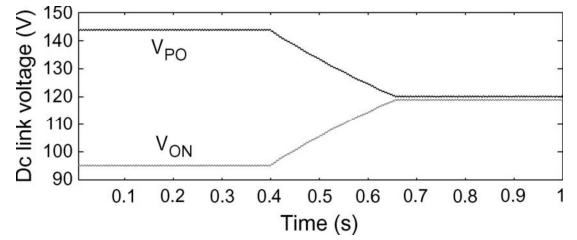Fig. 12. Block diagram for the dc link voltage control.

Fig. 13. Simulation results of the dc link voltage control.

for obtaining the results of Fig. 11 does not consider having the dc-link voltage control. The objective here is only to show that 3MV and 2MV1Z can have opposite behaviors in terms of charging the top capacitor, which is fundamental to the control task. Therefore, the opposite behavior of 3MV and 2MV1Z can be used to keep the balancing of capacitor voltages using the medium vectors. It can be seen that a RL load makes the dc link voltage control easier than the control with a resistive load.

In Fig. 12, the dc link voltage control is shown using the combination of 3MV and 2MV1Z. The idea is to generate a pulse with 1 or 0 changing each $60°$ and to apply a not exclusive-or (NXOR) with the result of the comparison between the reference (V_{PO}^*) and measured (V_{PO}) voltages. The output is used to enable the 3MV or the 2MV1Z.

To test the method, the system was simulated (Fig. 13) with $V_{PO}^* = 145$ V, $V_{ON}^* = 95$ V for the first part and $V_{PO}^* = 122$ V, $V_{ON}^* = 118$ V for the second part of the simulation. The parameters are equal to those used for simulation in Section V. It is noted that V_{PO} and V_{ON} follow the references and these voltages present ripple of 2 V, that is around 2% of the reference voltages, confirming the method efficiency.

The dc link voltage control is also confirmed through experimental measurements using the three-phase setup as shown in Fig. 1. The total voltage is kept in 240 V with $V_{PO}^* = 145$ V for the first part and $V_{PO}^* = 122$ V for the second part of the experiment (Fig. 14).

To analyze the effect of the proposed dc link voltage control on the maximum power point tracking performance, an array of 16 PV modules is considered for composing the dc link voltage, having two independent controls for each eight PV modules in series. In Fig. 15, it can be seen that the reference voltage only changes 20 V when the irradiance goes from 200 W/m² to 1000 W/m². The proposed scheme response is fast enough for implementing the maximum power point tracking since the dc link voltages follow the reference from 95 to 118 V in 400 ms
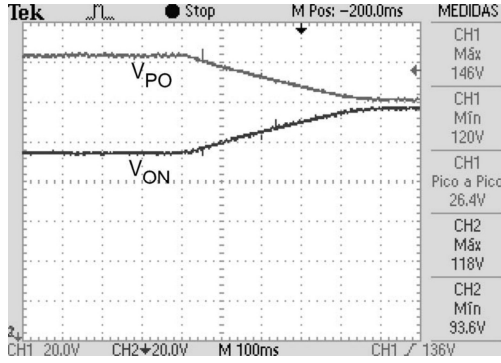
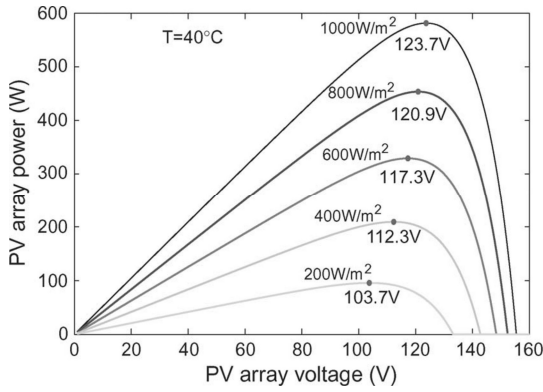Fig. 14. Experimental results of the dc link voltage control.

Fig. 15. PV array power with irradiance changes.

(Fig. 14). That would be equivalent to irradiance change from 100 W/m^2 to 650 W/m^2, which would take a much longer time to happen. Similar analysis can be done for temperature change.

VII. PHOTOVOLTAIC SYSTEM CONTROL WITH ADDITIONAL FUNCTION OF ACTIVE FILTER

The PV system control uses the p–q theory and requires the transformation of voltages and currents in *abc* coordinates to α–β–0 coordinates. With the voltages and currents determined in α–β–0 coordinates, the real power (p), imaginary power (q), and zero sequence power (p_0) can be calculated by using the p–q theory [13], [17]

$$\begin{bmatrix} p \\ q \\ p_0 \end{bmatrix} = \begin{bmatrix} v_\alpha & v_\beta & 0 \\ -v_\beta & v_\alpha & 0 \\ 0 & 0 & v_0 \end{bmatrix} \cdot \begin{bmatrix} i_\alpha \\ i_\beta \\ i_0 \end{bmatrix}. \quad (9)$$

The three-phase instantaneous power (p_3) corresponds to the sum of the instantaneous real power and the zero sequence power

$$p_3 = v_\alpha \cdot i_\alpha + v_\beta \cdot i_\beta + v_0 \cdot i_0 \quad (10)$$

$$= p + p_0. \quad (11)$$

It can be verified that p and q do not depend on the zero sequence voltage and current.

A. DC Link Voltage Control

The dc link voltage control aims to keep both capacitor voltages in adequate levels, allowing the inverter to work correctly. In addition to the components of instantaneous power defined by p–q theory, there are two other components, p_{reg1} and p_{reg2}, which are used to adjust the voltages of dc bus capacitors. In the NPC inverter, the dc link has two capacitors and the top capacitor is charged during the positive semi-cycle of the grid voltage, when it can absorb energy from the supply. The bottom capacitor is charged during the negative semi-cycle of the grid voltage. Therefore, two regulation powers p_{reg} are defined: one to charge the top capacitor in the positive semi-cycle of the grid voltage and the other to charge the bottom capacitor in the negative semi-cycle of the grid voltage. Each regulation power (p_{reg}) can be obtained using a proportional controller K_p

$$p_{reg_1} = K_p \cdot (v_{ref} - V_{dc_1}) \quad (12)$$

$$p_{reg_2} = K_p \cdot (v_{ref} - V_{dc_2}) \quad (13)$$

where:

K_p proportional gain;
v_{ref} reference voltage;
V_{dc_1} top capacitor measured voltage;
V_{dc_2} bottom capacitor measured voltage.

The total regulation power p_{reg} is

$$p_{reg} = p_{reg_1} + p_{reg_2} \quad (14)$$

where p_{reg_1} only exists in the positive semi-cycle and p_{reg_2} in the negative semi-cycle of the grid voltage. Therefore, when one exists, the other is null. p_{reg} is included with negative signal in the value of real power to be delivered by the converter to the ac mains (p_x)

$$p_x = \tilde{p} - \bar{p}_0 - p_{reg} \quad (15)$$

$$q_x = q \quad (16)$$

where $\tilde{p}$ is the alternating value of the real power and $\bar{p}_0$ is the average value of the zero sequence power.

B. Current Control

The reference power components p_x and q_x are used to calculate the compensation currents in α–β–0 coordinates by the expression

$$\begin{bmatrix} i_{F\alpha}^* \\ i_{F\beta}^* \end{bmatrix} = \frac{1}{v_\alpha^2 + v_\beta^2} \cdot \begin{bmatrix} v_\alpha & -v_\beta \\ v_\beta & v_\alpha \end{bmatrix} \cdot \begin{bmatrix} p_x \\ q_x \end{bmatrix} \quad (17)$$

$$i_{F0}^* = i_0 = \frac{1}{\sqrt{3}} \cdot (i_a + i_b + i_c). \quad (18)$$

Equation (17) is valid when there is no zero sequence power, allowing to select the compensation value (p_0, $\bar{p}_0$, and $\tilde{p}_0$ or even a part of these powers). The block diagram of the control system is presented in Fig. 16. The filter to obtain the oscillating
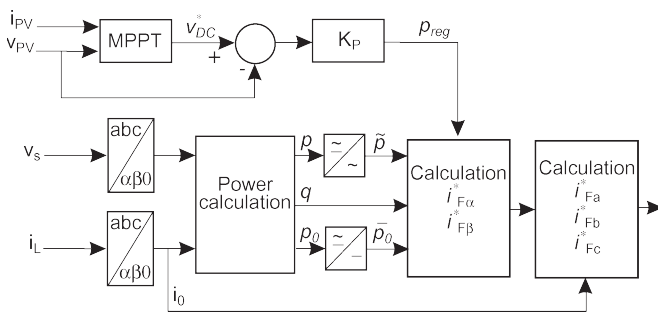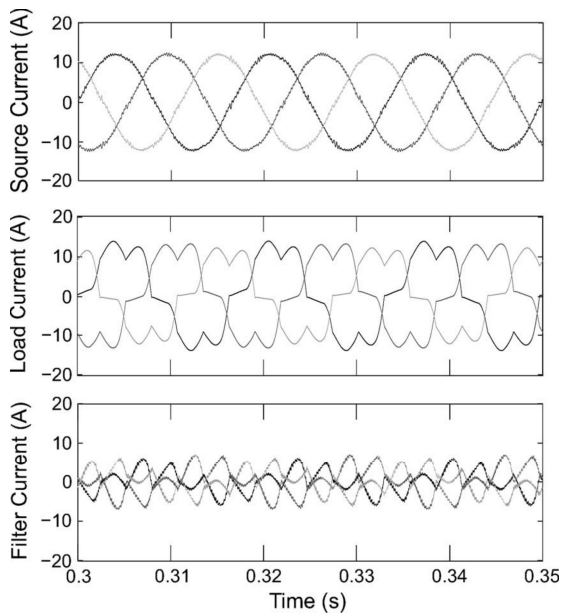
Fig. 16.   Block diagram of the control system.

Fig. 17.   Simulation results for the currents: (a) source, (b) load, and (c) filter.

part of p is a second order filter with cut frequency of 6 Hz [19] and the dc part of p_0 is considered zero.

C. Simulation Results

The proposed control system with function of active filter using the p–q theory discussed is applied to the three-phase NPC connected to the grid. The simulation conditions are switching period $T_s = 200$ μs, dead time $t_d = 3.5$ μs, rms source voltage $V_S = 64$ V source frequency $f = 60$ Hz, source inductance $L_S = 1.2$ mH, filter inductance $L_f = 1.8$ mH, dc link capacitance $C = 2.35$ mF, and dc link voltage $V_{PN} = 240$ V. The load is composed of two components: linear and nonlinear. Each phase of the linear component is made of one inductance (9.6 mH) in series with one resistance. The resistances of each phase are different (16 Ω, 48 Ω, and 121 Ω) to prove the load capability balancing of the AF function. The nonlinear load is composed of a three-phase rectifier with $C = 306$ μF and $R = 15$ Ω in parallel (dc side). The measured source (i_S), load (i_L), and filter (i_F) currents are presented in Fig. 17. The harmonic spectrum of the source current is shown in Fig. 18(a) without harmonic compensation and the Fig. 18(b) shows the same current with harmonic compensation, proving the capability of the AF.
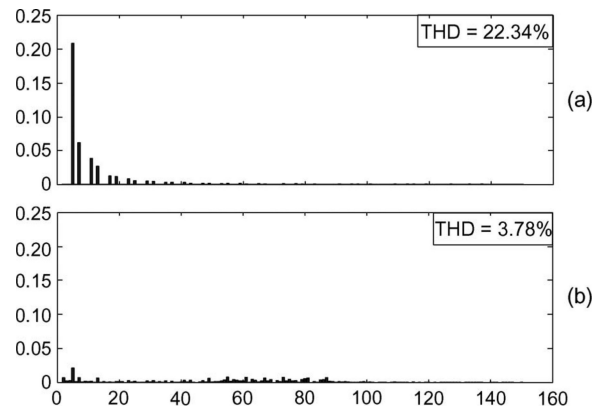

Fig. 18.   Harmonic spectrum of the source and load currents without showing the fundamental frequency.

VIII. CONCLUSION

In this paper, modulation techniques designed for three-phase transformerless photovoltaic systems are proposed. The techniques guarantee constant common-mode voltage, improving the behavior of the neutral point clamped inverter in terms of leakage currents without additional hardware. For achieving constant common-mode voltage, the inverter switches are controlled by using only medium vectors and one specific zero vector. Three possibilities of modulation are described. Simulation and experimental results of the neutral point clamped inverter are presented to validate the theoretical models. To increase the three-phase transformerless photovoltaic system utilization, the control is designed for performing the additional function of active filter using the p–q theory.

REFERENCES

[1] F. Blaabjerg, R. Teodorescu, M. Liserre, and A. V. Timbus, "Overview of control and grid synchronization for distributed power generation systems," *IEEE Trans. Ind. Electron.*, vol. 53, no. 5, pp. 1398–1409, Oct. 2006.

[2] M. Liserre, A. Pigazo, A. Dell'Aquila, and V. M. Moreno, "An anti-islanding method for single-phase inverters based on a grid voltage sensorless control," *IEEE Trans. Ind. Electron.*, vol. 53, no. 5, pp. 1418–1426, Oct. 2006.

[3] F. Blaabjerg, Z. Chen, and S. B. Kjaer, "Power electronics as efficient interface in dispersed power generation systems," *IEEE Trans. Power Electron.*, vol. 19, no. 5, pp. 1184–1194, Sep. 2004.

[4] E. Gubía, P. Sanchis, A. Ursúa, J. López, and L. Marroyo, "Ground currents in single-phase transformerless photovoltaic systems," *Prog. Photovolt., Res. Appl.*, vol. 15, no. 7, pp. 629–650, Nov. 2007.

[5] S. B. Kjaer, J. K. Pedersen, and F. Blaabjerg, "A review of single-phase grid-connected inverters for photovoltaic modules," *IEEE Trans. Ind. Appl.*, vol. 41, no. 5, pp. 1292–1306, Sep./Oct. 2005.

[6] M. García, J. M. Maruri, L. Marroyo, E. Lorenzo, and M. Pérez, "Partial shadowing, MPPT performance and inverter configurations: Observations at tracking PV plants," *Prog. Photovolt., Res. Appl.*, vol. 16, no. 6, pp. 529–536, Sep. 2008.

[7] P. Sanchis, J. López, A. Ursúa, E. Gubía, and L. Marroyo, "On the testing, characterization, and evaluation of PV inverters and dynamic MPPT performance under real varying operating conditions," *Prog. Photovolt., Res. Appl.*, vol. 15, no. 6, pp. 541–556, Sep. 2007.

[8] S. Busquets-Monge, J. Rocabert, P. Rodriguez, S. Alepuz, and J. Bordonau, "Multilevel diode-clamped converter for photovoltaic generators with independent voltage control of each solar array," *IEEE Trans. Ind. Electron.*, vol. 55, no. 7, pp. 2713–2723, Jul. 2008.

[9] M. C. Cavalcanti, K. C. Oliveira, A. M. Farias, F. A. S. Neves, G. M. Azevedo, and F. C. Camboim, "Modulation techniques to eliminate leakage currents in transformerless three-phase photovoltaic systems," *IEEE Trans. Ind. Electron.*, vol. 57, no. 4, pp. 1360–1368, Apr. 2010.

[10] R. Gonzalez, E. Gubia, J. Lopez, and L. Marroyo, "Transformerless single-phase multilevel-based photovoltaic inverter," *IEEE Trans. Ind. Electron.*, vol. 55, no. 7, pp. 2694–2702, Jul. 2008.

[11] S. Daher, J. Schmid, and F. L. M. Antunes, "Multilevel inverter topologies for stand-alone PV systems," *IEEE Trans. Ind. Electron.*, vol. 55, no. 7, pp. 2703–2712, Jul. 2008.

[12] B. Singh, K. Al-Haddad, and A. Chandra, "A review of active filters for power quality improvement," *IEEE Trans. Ind. Electron.*, vol. 46, no. 5, pp. 960–971, Nov. 1999.

[13] H. Akagi, Y. Kanazawa, and A. Nabae, "Instantaneous reactive power compensator comprising switching devices without energy storage components," *IEEE Trans. Ind. Appl.*, vol. IA-20, no. 3, pp. 625–630, May/Jun. 1984.

[14] E. H. Watanabe, R. M. Stephan, and M. Aredes, "New concepts of instantaneous active and reactive powers in electrical systems with generic loads," *IEEE Trans. Power Del.*, vol. 8, no. 2, pp. 697–703, Apr. 1993.

[15] M. Aredes and E. H. Watanabe, "New control algorithm for series and shunt three-phase four-wire active power filters," *IEEE Trans. Power Del.*, vol. 10, no. 3, pp. 1619–1656, Jul. 1995.

[16] J. Leon, S. Vazquez, J. Sanchez, R. Portillo, L. Franquelo, J. Carrasco, and E. Dominguez, "Conventional space-vector modulation techniques versus the single-phase modulator for multilevel converters," *IEEE Trans. Ind. Electron.*, vol. 57, no. 7, pp. 2473–2482, Jul. 2010.

[17] J. L. Afonso, M. J. S. Freitas, and J. S. Martins, "P-q theory power components calculations," in *Proc. IEEE Int. Symp. Ind. Electron.*, Jun. 2003, pp. 385–390.

[18] J. Liu, J. Yang, and Z. Wang, "A new approach for single-phase harmonic current detecting and its application in a hybrid active power filter," in *Proc. IEEE IECON*, Jul. 1999, pp. 849–854.

[19] R. I. Bojoi, G. Griva, V. Bostan, M. Guerriero, F. Farina, and F. Profumo, "Current control strategy for power conditioners using sinusoidal signal integrators in synchronous reference frame," *IEEE Trans. Power Electron.*, vol. 20, no. 6, pp. 1402–1412, Nov. 2005.

Marcelo C. Cavalcanti was born in Recife, Brazil, in 1972. He received the B.S. degree in electrical engineering from the Federal University of Pernambuco, Recife, Brazil, in 1997, and the M.S. and Ph.D. degrees in electrical engineering from the Federal University of Campina Grande, Campina Grande, Brazil, in 1999 and 2003, respectively.

Since 2003, he has been at the Department of Electrical Engineering, Federal University of Pernambuco, where he is currently a Professor of Electrical Engineering. His research interests are renewable systems and power quality.

Alexandre M. Farias (S'09) was born in Recife, Brazil, in 1983. He received the B.S. and M.S. degrees in electrical engineering from the Federal University of Pernambuco, Recife, Brazil, in 2008 and 2011, respectively, where he is currently working toward the Ph.D. degree.

His research interests are renewable systems and power quality.

Kleber C. Oliveira was born in Recife, Brazil, in 1980. He received the B.S. and M.S. degrees in electrical engineering from the Federal University of Pernambuco, Recife, Brazil, in 2005 and 2007, respectively, where he is currently working toward the Ph.D. degree.

He worked as a Visiting Scholar at the University of Minho, Guimarães, Portugal, from Mar. 2009 to Dec. 2009. He is currently at Professor at the University of Pernambuco (UPE). His research interests are renewable systems and power quality.

Francisco A. S. Neves (M'00) was born in Campina Grande, Brazil, in 1963. He received the B.S. and M.Sc. degrees in electrical engineering from the Federal University of Pernambuco, Recife, Brazil, in 1984 and 1992, respectively, and the Ph.D. degree in electrical engineering from the Federal University of Minas Gerais, Belo Horizonte, Brazil, in 1999.

He worked as a visiting scholar at Georgia Institute of Technology, Atlanta, during 1999, and at Alcala University, Alcalá de Henares, Spain, from Feb. 2008 to Jan. 2009. Since 1993, he has been with the Department of Electrical Engineering, Federal University of Pernambuco, where he is currently a Professor of Electrical Engineering. His research interests include power electronics, renewable energy systems, power quality and grid synchronization methods.

João L. Afonso (M'00) was born in Rio de Janeiro, Brazil, on 1963. He received the degree in electrical engineering and the M.Sc. degree in electrical engineering from the Federal University of Rio de Janeiro, Rio de Janeiro, Brazil, in 1986 and 1991, respectively, and the Ph.D. degree in industrial electronics from the University of Minho, Guimarães, Portugal, in 2000.

He is Associate Professor at the Department of Industrial Electronics of the University of Minho, Portugal, where he works since 1993. He lectures the subjects of Electrical Machines, Complements of Power Electronics, Electrical Power Quality, Active Power Filters, and Renewable Energy. His researching activities are related with the development of Active Power Filters, Power Quality Monitoring Systems, Power Electronics for Renewable Energy Sources and for Electric Vehicles, and with the realization of studies on Power Quality and Energy Efficiency.